Journal of Hazardous Materials 317 (2016) 246–258

Contents lists available at ScienceDirect

Journal of Hazardous Materials

journal homepage: www.elsevier.com/locate/jhazmat

Influence of pH, layer charge location and crystal thickness distribution on U(VI) sorption onto heterogeneous dioctahedral smectite

Vanessa Guimarães[a,c], Enrique Rodríguez-Castellón[b], Manuel Algarra[b], Fernando Rocha[c], Iuliu Bobos[a,*]

[a] Instituto de Ciências da Terra – Porto, DGAOT, Faculdade de Ciências, Universidade do Porto, Rua do Campo Alegre 687, 4169-007 Porto, Portugal
[b] Departamento de Química Inorgánica, Facultad de Ciencias, Universidad de Málaga. Campus de Teatino s/n, 29071 Málaga, Spain
[c] Geobiotec. Departamento de Geociências da Universidade de Aveiro, Campo Universitário de Santiago, 3810-193 Aveiro, Portugal

HIGHLIGHTS

- The UO_2^{2+} sorption at pH 4 and 6 on heterogeneous smectite structure.
- The cation exchange process is affected by layer charge distribution.
- Surface complexation and cation exchange modelling.
- New binding energy components identified by X-ray photoelectron spectroscopy.

ARTICLE INFO

Article history:
Received 20 January 2016
Received in revised form 4 May 2016
Accepted 19 May 2016
Available online 20 May 2016

Keywords:
Heterogeneous smectite structure
Crystal thickness
Batch sorption experiments
Uranyl surface complexation
X-ray photoelectron spectroscopy

ABSTRACT

The UO_2^{2+} adsorption on smectite (samples BA1, PS2 and PS3) with a heterogeneous structure was investigated at pH 4 (I = 0.02 M) and pH 6 (I = 0.2 M) in batch experiments, with the aim to evaluate the influence of pH, layer charge location and crystal thickness distribution. Mean crystal thickness distribution of smectite crystallite used in sorption experiments range from 4.8 nm (sample PS2), to 5.1 nm (sample PS3) and, to 7.4 nm (sample BA1). Smaller crystallites have higher total surface area and sorption capacity. Octahedral charge location favor higher sorption capacity. The sorption isotherms of Freundlich, Langmuir and SIPS were used to model the sorption experiments. The surface complexation and cation exchange reactions were modeled using PHREEQC-code to describe the UO_2^{2+} sorption on smectite. The amount of UO_2^{2+} adsorbed on smectite samples decreased significantly at pH 6 and higher ionic strength, where the sorption mechanism was restricted to the edge sites of smectite. Two binding energy components at 380.8 ± 0.3 and 382.2 ± 0.3 eV, assigned to hydrated UO_2^{2+} adsorbed by cation exchange and by inner-sphere complexation on the external sites at pH 4, were identified after the U4$f_{7/2}$ peak deconvolution by X-photoelectron spectroscopy. Also, two new binding energy components at 380.3 ± 0.3 and 381.8 ± 0.3 eV assigned to $\equiv AlOUO_2^+$ and $\equiv SiOUO_2^+$ surface species were observed at pH 6.

1. Introduction

Smectite clay is widely used as "buffer" barrier in engineered radioactive waste containment systems, owing to their low permeability and high sorption capacity [1]. The performance of the engineering barrier in a high-level waste repository is highly affected by structural changes caused by alteration of the original smectite [2,3]. The effect of temperature is reflected by increase of smectite surface charge, induced by silica for aluminium substitution in the tetrahedral sheet, affecting also the cation exchange capacity (CEC) and their swelling properties [4–8].

Long-term smectite stability after waste emplacement is low because buffer material will be exposed to a maximum temperature of 150 °C at the surface of the waste package, pressure in the range of 100–300 bars and groundwaters of various compositions depending to the geological environment [9]. Detailed studies of the reactivity of dioctahedral smectite have shown that the hydrothermal conditions imply the formation of high- and low-charge layers

* Corresponding author.
E-mail address: ibobos@fc.up.pt (I. Bobos).

http://dx.doi.org/10.1016/j.jhazmat.2016.05.060
0304-3894/

in different proportions on smectite [10] and the progressive formation of illite-montmorillonite mixed layers [11,12].

Uranium (U) occurs as uranyl (UO_2^{2+}) ions under oxidizing geochemical conditions and acidic aqueous solutions, forming monomers, dimers, and trimers at higher pH hydrolyses [13]. The pH dependent adsorption behaviour under these conditions is similar to other metal oxides with a cationic adsorption on edge sites at pH 5–6 and an additional anionic adsorption on edge sites around pH 8 in systems equilibrated with atmospheric CO_2 [14]. Despite the importance of this mechanism, there is a limited knowledge about the interactions between UO_2^{2+} ions and clay mineral surfaces [15]. The interaction of UO_2^{2+} ions with clay minerals as potential adsorbent materials with high surface area were carried out with montmorillonite [14,16–28], tri-smectite [29–31] or bentonite rocks [32].

Uranyl sorption onto smectite involves multiple binding sites, including ion exchange and edge surface sites. Previous works reported that the adsorption of UO_2^{2+} on smectite follows two main mechanisms: ion-exchange through outer-sphere complexation at low pH and low ionic strength, whereas at near-neutral pH and high ionic strength through inner-sphere complexation on the edge sites controls the sorption mechanism [14,18,26,29,31,33,34].

The development of surface complexation models (SCM) predicts the behavior of uranyl sorption on different clay minerals by fitting the thermodynamic data obtained from reference methods under different environmental conditions [35–37]. The use of a "unique model" was developed to defend the standardization of SCM using thermodynamic approaches and parameter optimization in order to achieve the best fit to the experimental sorption data [22,37–39]. In this way, it was possible to reduce the number of adjustable parameters and provide a set of uniform parameters based on common reference values.

The main aim of this study is to understand the degree of interaction between UO_2^{2+} and dioctahedral smectite with a heterogeneous structure as a function of layer charge location and the type of interstratified layers, in order to predict the possible changes on sorption mechanism caused by structural modification of smectite during alteration. The heterogeneous smectite structure used in sorption experiments represents in fact the first alteration stage of smectite exposed to circulation of hydrothermal fluids or as backfilling materials in nuclear waste disposal [2].

The kinetic of sorption-desorption experiments of the UO_2^{2+} retardation onto heterogeneous smectite samples using a continuous stirred tank reactor was previously interpreted by the reaction-controlled model (pseudo-first order and pseudo-second order) and diffusion-controlled model (intra-particle diffusion and liquid-film diffusion) [40]. The adsorption experiments in this work were carried out to evaluate the role of pH, charge location and the crystal thickness distribution of smectite on the UO_2^{2+} sorption mechanism. The pH variation influences the UO_2^{2+} aqueous speciation defining the species involved during the sorption mechanism. Also, it may play an important role in the surface sites distribution, controlling the adsorption capacity and the binding strength of surface complexes. The adsorption process on different smectite samples was simulated using the cation exchange and surface complexation model based on diffuse double layer (DDL) [41]. The UO_2^{2+} surface species adsorbed on smectite at pH 4 and pH 6 were also identified by X-ray photoelectron spectroscopy (XPS) experiments.

2. Experimental

2.1. Batch experiments

Batch experiments were carried out to investigate the UO_2^{2+} adsorption on three different heterogeneous smectites (<2 μm fractions), with a different distribution of charge deficit. The adsorption experiments were carried out at pH 4 and 6, using low (I = 0.02 M) and high ionic strength (I = 0.2 M), in order to promote the study of both sorption mechanisms on smectite surface: ion exchange and inner-sphere complexation on the surface edge sites. Batch experiments performed at pH = 4 were carried out by adding 0.025 g of the respective clay mineral with 14.00 mL (S: L = 1.79 g/L) of different stock solutions at different UO_2^{2+} concentrations, ranged between 1.00×10^{-5} M and 6.50×10^{-4} M, with NaCl (0.02 M). At pH = 6, 0.050 g (S: L = 3.60 g/L) of each smectite was added, and the UO_2^{2+} concentration of stock solutions ranged between 1.00×10^{-6} M and 1.00×10^{-4}M, with NaCl (0.2 M). Suspensions were shaken for 48 h, and then centrifuged, separated and the resulted (supernatant) solutions were preserved by adding HCl and stored at 4 °C for subsequent chemical analysis. Uranyl stock solutions were prepared from a primary standard solution (1.0×10^{-3} M), obtained by dissolving of $UO_2(CH_3COO)_2 \times 2H_2O$ in deionized water. The pH was adjusted to the required value and monitored with NaOH (0.05 M) or HCl (0.05 M) (Merck, Germany), using a pH meter (Corning 240) calibrated with buffer solutions (pH 4, 7 and 10, Merck).

2.2. Isothermal models

The Langmuir model assumes that the sorption sites are identical and energetically equivalent due to its homogeneous structure [42]. The equilibrium is obtained when the monolayer formation on the sorbent occurs. Langmuir isotherm is described according to the following Eq. (1):

$$q_e = \frac{q_m K_L C_e}{(1 + K_L C_e)} \quad (1)$$

where q_e (mol/kg) and C_e (mol/L) are the equilibrium concentrations of UO_2^{2+} in the solid and the liquid phase, respectively, q_m (mol/kg) is the maximum sorption capacity, and K_L (L/kg) is the Langmuir constant related to the energy of adsorption. The q_e is obtained according to Eq. (2):

$$q_e = (C_i - C_f)\frac{V}{m} \quad (2)$$

where C_i and C_f are the concentrations of UO_2^{2+} in the beginning and the end of the adsorption process, V is the solution volume used during batch experiments (14.00 mL) and m is the mass of smectite used.

Freundlich model was used to describe the adsorption of contaminants on heterogeneous surface consisting of sites with different exponential distribution and energies [43,44]. The equation of the Freundlich sorption isotherm is expressed by Eq. (3):

$$q_e = K_F C_e^{\,n} \quad (3)$$

where, K_F and n are the Freundlich adsorption isotherm constants, being indicative of the adsorption extension and the degree of the surface heterogeneity. The Sips isotherm combines both Freundlich and Langmuir isotherms where at low adsorbate concentration behaves as Freundlich isotherm, whereas at high concentration predicts a monolayer adsorption capacity characteristic to Langmuir model [45,46]. The mathematical representation of this model is given by Eq. (4):

$$q_e = \frac{q_m (K_S C_e)^n}{1 + (K_S C_e)^n} \quad (4)$$

where, q_m (mol/kg) is the maximum sorption capacity, which can also be expressed as Nt, a measure of the total number of binding sites available per g of sorbent, K_S is the affinity constant for adsorption (L/kg) and n is the Freundlich parameter that takes into account the system heterogeneity. The Sips isotherm is reduced to

the Langmuir form for n = 1 and a homogeneous surface is considered. The greater is the difference from this value, the greater will be the clay surface heterogeneity.

2.3. Diffuse double layer surface complexation and cation exchange modelling

The diffuse double layer surface complexation model was used to predict the UO_2^{2+} surface complexation reactions onto smectite. The PHREEQC-code [41] describes the surface complexation model including a combination of equilibrium protonation ($\equiv SOH_2^+$), deprotonation ($\equiv SO^-$) and complexation reactions based on previous UO_2^{2+} sorption experiments on montmorillonite [23]. This process was based on the geochemical code proposed by [47]. The major surface reactions and input parameters included in our model are resumed in Table 2. The second geochemical code developed on PHREEQC was additionally used to describe the cation exchange process of UO_2^{2+} adsorption at pH 4 and pH 6 [41]. The cation exchange on the permanently charged planar sites (Eq. (5)) was modeled taking into account the adsorbent CEC ($eqkg^{-1}$) and the selectivity coefficient for each ion exchange process occurring on the planar sites, given by Eq. (6) [48].

$$bA^a - Clay + aB^b \leftrightarrow aB^b - Clay + bA^a \quad (5)$$

$${}^{B}_{A}K_c = \frac{N_B^a}{N_A^b} \times \frac{A^b}{B^a} \times \frac{\gamma_A^b}{\gamma_B^a} \quad (6)$$

The selectivity constants used to model UO_2^{2+} exchange process are resumed in Table 2. The selectivity coefficient (K_c) regarding to the exchange process between UO_2^{2+} and Ca^{2+} ($^{UO_2}_{Ca}K_c$), was obtained from the ratio $^{UO_2}_{Na}K_c/^{Ca}_{Na}K_c$ [22,49,50].

The proportion of Ca^{2+} and Na^+ from smectite was taken into account (Table 2) in the modelling of cation exchange process. Therefore, two different exchange master species were defined according to the next geochemical code developed on PHREEQC:

"EXCHANGE MASTER SPECIES

XX-#Na-Smectite

ZZ-#Ca-Smectite

EXCHANGE_SPECIES

$X^- = X^-$; log_k 0.0

$Z^- = Z^-$; log_k 0.0

$X^- + Na^+ = NaX$; log_k 0.0

$2X^- + UO_2^{+2} = UO_2^{+2} \times 2$; logk 0.45

$2Z^- + UO_2^{+2} = UO_2^{+2}Z_2$; logk 0.049

$Z^- + Na^+ = NaZ$; log_k 0.23

SOLUTION1

pH4.3

Na^+20 #concentrations in mmol/kgH_2O

U(6) 7.36e-1

Acetate 1.47

Cl 20 charge

EXCHANGE

X 1.14e-4#13% Na^+

Z 7.43e-4#87% Ca^{2+}

-equilibrate 1″

The permanent charged sites ($\equiv X^-$) was estimated to be equal with the cation exchange capacity, whereas the reactive edge sites capacity was assumed to be 15% of the total number of crystallite edge sites available. The edge surface sites may correspond to 10–20% of the total number of sites available for sorption [51]. It was also defined that the ratio between ≡AlOH and ≡SiOH sites is 0.83 for smectite [52]. The aqueous speciation equilibrium constants (log K) considered in our model were obtained from NEA uranium thermodynamic database [53,54].

A combination of four surface complexes, $\equiv AlOUO_2^+$, $\equiv AlO(UO_2)_3(OH)_5$, $\equiv SiOUO_2^+$ and $\equiv AlO(UO_2)_3(OH)_5$, was assumed for a best prediction of the experimental sorption data [23]. The chemical modeling program FITEQL 4.0 [55] was used to optimize the respective surface complexation constants using the DDL model by means of fitting the UO_2^{2+} sorption data from pH 4 to pH

Table 1
Crystal chemistry and physico-chemical properties of clay minerals.

Sample	Structural Formula	*T*(nm)	S_{BET} (m^2/g)	CEC (meq/g)	Charge Def./Uc	Na/Ca
BA1	$Ca_{0.27}Na_{0.20}(Al_{1.30}Fe_{0.36}Mg_{0.33})(Si_{3.63}Al_{0.37})O_{10}(OH)_2$	7.4	12	0.96	− 1.38 48%O 52%T − 1.31	0.74
PS2	$Ca_{0.14}Na_{0.38}K_{0.08}(Al_{1.25}Fe_{0.34}Mg_{0.39})(Si_{3.74}Al_{0.26})O_{10}(OH)_2$	4.8	26	1.04	62%O 38%T − 1.45	2.71
PS3	$Ca_{0.15}Na_{0.30}K_{0.14}(Al_{1.17}Fe_{0.41}Mg_{0.42})(Si_{3.70}Al_{0.30})O_{10}(OH)_2$	5.1	84	0.81	59%O 41%T	2.00
SW1[a]	$Ca_{0.12}Na_{0.32}K_{0.05}(Al_{1.50}Fe_{0.21}Mg_{0.27}Ti_{0.01})(Si_{3.99}Al_{0.01})O_{10}(OH)_2$	8.1	31.82	0.76		
SBId1[b]	$Ca_{0.05}Na_{0.12}K_{0.16}(Al_{1.78}Fe_{1.04}Mg_{0.46}Ti_{0.49})(Si_{3.77}Al_{0.23})O_{10}(OH)_2$	12.3				

[a] Na-Montmorillonite, Wyoming, Source: Clay Minerals Society Repository.
[b] Beidellite Black Jack, Idaho, Source: Clay Minerals Society Repository.

Table 2
Model parameters used to simulate the UO_2^{2+} adsorption on smectite.

Model conditions	Samples		
	BA1	PS2	PS3
Solid concentration (S:L) (g/L)	3.60 (pH 6) 1.79 (pH4)		
Surface area (BET) (m^2/g)	12	26	82
Total site concentration (mol/kg)	0.084	0.092	0.071
Edge site reactions	Log K		
$\equiv AlOH + H^+ = \equiv AlOH_2^+$	12.30[a]	12.30[a]	12.30[a]
$\equiv AlOH = \equiv AlO^- + H^+$	−13.60[a]	−13.60[a]	−13.60[a]
$\equiv AlOH + UO_2^{2+} = \equiv AlOUO_2^+ + H^+$	7.70[b]	7.94[b]	7.84[b]
$\equiv AlOH + 3UO_2^{2+} + 5H_2O = \equiv AlO(UO_2)_3(OH)_5 + H^+$	−15.19[b]	−14.95[b]	−15.06[b]
$\equiv AlOH + Na^+ = \equiv AlONa + H^+$	−6.60	−6.60	−6.60
$\equiv SiOH = \equiv SiO^- + H^+$	−6.95[a]	−6.95[a]	−6.95[a]
$\equiv SiOH + UO_2^{2+} = \equiv SiOUO_2^+ + H^+$	0.75[b]	0.99[b]	0.89[b]
$\equiv SiOH + 3UO_2^{2+} + 5H_2O = \equiv SiO(UO_2)_3(OH)_5 + H^+$	−16.19[b]	−15.95[b]	−16.06[b]
$\equiv SiOH + Na^+ = \equiv SiONa + H^+$	−10.37	−10.37	−10.37
Exchange reactions	Selectivity coefficient (K_c)[c]		
$2Na^+$-clay + $UO_2^{2+} \leftrightarrow UO_2^{2+}$-clay + $2Na^+$	2.82 (Na^+-13%)	2.82 (Na^+-87%)	2.82 (Na^+-65%)
$2Na^+$-clay + $Ca^{2+} \leftrightarrow Ca^{2+}$-clay + $2Na^+$	2.50	2.50	2.50
Ca^{2+}-clay + $UO_2^{2+} \leftrightarrow UO_2^{2+}$-clay + Ca^{2+}	1.12	1.12	1.12
Ca^{2+}-clay + $2Na^+ \leftrightarrow Na_2$-clay + Ca^{2+}	1.70 (Ca^{+2}-87%)	1.70(Ca^{+2}-13%)	1.70(Ca^{+2}-35%)
Aqueous Speciation			
$UO_2^{2+} + H_2O = UO_2(OH)^+$	−5.25[d]		
$2UO_2^{2+} + 2H_2O = (UO_2)_2(OH)_2^{2+} + 2H^+$	−5.62[d]		
$3UO_2^{2+} + 5H_2O = (UO_2)_3(OH)_5^+ + 5H^+$	−15.55[d]		
$UO_2^{2+} + 3(H_2O) = UO_2(OH)_3^- + 3H^+$	−20.25[d]		

[a] McKinley et al. (1995).
[b] Fitted binding constants.
[c] Calculated selectivity coefficient.
[d] Guillaumont et al. (2003).

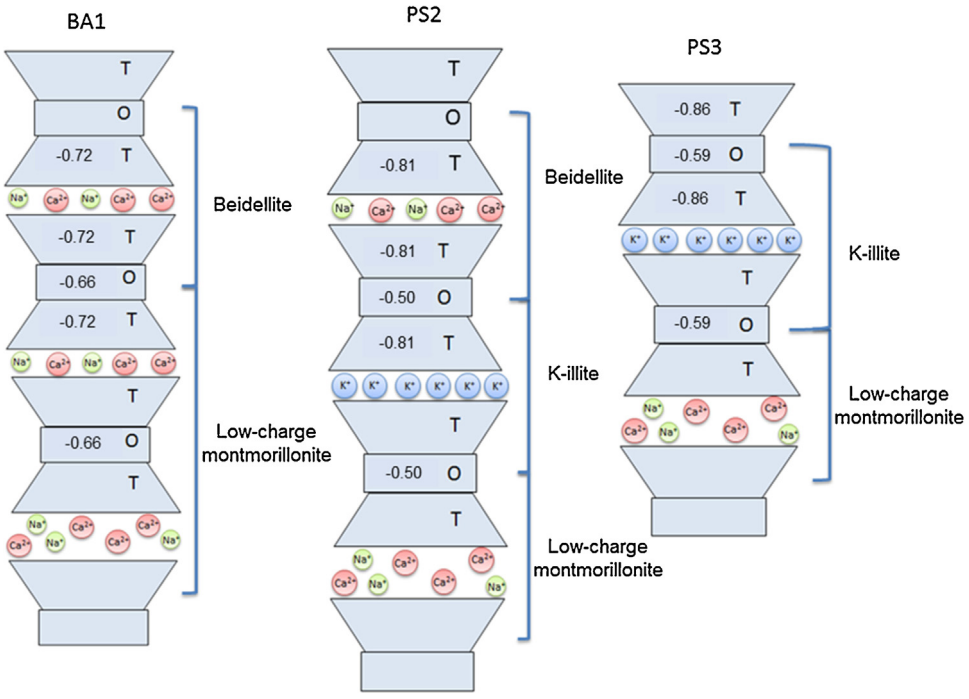

Fig. 1. Idealization of smectite structure: (a) BA1 sample corresponding to beidellite and low-charge montmorillonite interstratified structure; (b) PS2 sample of beidellite, illite and low-charge montmorillonite interstratified structure; (c) PS3 sample composed by illite and low-charge montmorillonite interstratified structure.

7, using a concentration of UO_2^{2+} of 1.0×10^{-4}M and 0.2 M of NaCl. Fig. 2 shows the comparison between the U(VI) sorption data on BA1, PS2 and PS3 smectite samples and the surface complexation model. The respective binding constants were then used in the PHREEQC-code in order to predict the amount of UO_2^{2+} adsorbed for different initial concentrations of UO_2^{2+}, different pH conditions and ionic strengths. In this way, different solutions were defined in the PHREEQC-code in order to simulate the isothermal curves.

In the presence of CO_2 (g) atmospheric, the UO_2^{2+} adsorption on smectite is affected at pH > 6.5 with the formation of uranyl-carbonate ternary-surface complexes. These surface complexation

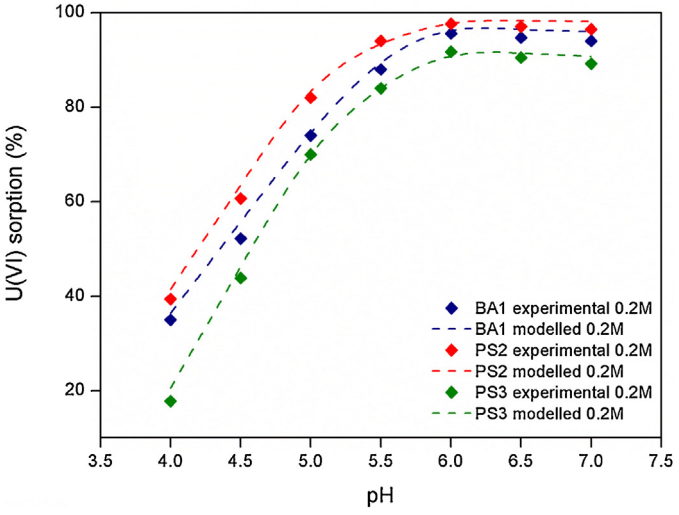

Fig. 2. Comparison of UO_2^{2+} sorption data on heterogeneous smectite samples (BA1, PS2 and PS3) and the surface complexation model (FITEQL). $[UO_2^{2+}] = 1.00 \times 10^{-4}$ M, S:L = 3.60, $P_{CO2} = 10^{-3.5}$ Pa, 25 °C, I = 0.2 M.

reactions were not included in our model, restricting their efficiency to the adsorption experiments occurring from acidic to near-neutral pH conditions. The root mean square error (RMSE) given by Eq. (5) [56] was used to measure the difference between both models:

$$RMSE(\%) = \sqrt{\frac{\sum_{i=1}^{n}\left(x_{1,i} - x_{2,i}\right)^2}{n}} \times 100 \quad (7)$$

where $x_{1,i}$ and $x_{2,i}$ are the measured and calculated amounts of UO_2^{2+} adsorbed on smectite, respectively, and n is the total number of experiments carried out using different UO_2^{2+} concentrations.

3. Results and discussion

3.1. Crystal thickness distribution

The physical and chemical properties (i.e., surface area, CEC, sorption, solubility, etc) of a clay mineral may be strongly influence by crystal thickness or particle size distribution. Mean crystal thickness (T) of smectite crystals used in our experiments is 4.8 and 5.1 nm for samples PS2 and PS3, and 7.4 nm for sample BA1 (Table 1). The T (nm) corresponding to Na-montmorillonite SW1 and beidellite Black Jack were compared with our data (Table 1).

The T values obtained were used for calculation the total surface area (TSA) which includes the basal interfaces and edges of crystals using the following equation: TSA = 100/0.12 T [57]. The values obtained (Table 1) show that the smaller crystals have higher TSA.

3.2. Effect of layer charge location and heterogeneous layers distribution

The effect of layer charge distribution between tetrahedral and/or octahedral sheets of smectite was taken into account in sorption experiment. Different charge layers reveal different smectite layers compositions regarding to the degree of octahedral and tetrahedral substitutions. Also, the influence of charge distribution of selected smectite samples was evaluated taking into account the ratio between the CEC values and the respective layer charge deficits (Table 1).

Higher proportions of tetrahedral substitution ($-0.37/(Si,Al)_4O_{10}$) attributed to beidellite layers correspond to sample BA1, whereas the lower tetrahedral charge deficit and the higher proportion of octahedral substitution occur in samples PS2 ($-0.26/(Si,Al)_4O_{10}$) and PS3 ($-0.30/(Si,Al)_4O_{10}$). Reduced interlayer distances induced by the increase of layer substitutions and by the proximity between the charge deficit of tetrahedral sheet and the contaminant, restrict the ion-exchanges process hampering the UO_2^{2+} uptake. In this way, sample BA1 has higher charge than PS2 but lower CEC value (Table 1).

A hypothetic structure of smectite samples used in sorption experiments is shown in Fig. 1, where both layer-types and charge layers are shown for each smectite sample used in sorption experiments according to the structural and chemical data obtained by XRD and EMPA.

The lower proportion of tetrahedral substitutions of PS2 improved the adsorption on interlayer sites, contrary to what is observed for sample PS3 (CEC = 0.81 meq/g). Usually, a decrease of CEC occurs as the percentage of illite layers increases in the randomly interstratified structure of I/S formed. Sample PS3 has the higher proportion of illite interstratified layers (≈30%), the lower number of available sites for ion-exchange and a randomly 2W/1 W smectite that favoured the decrease of contaminant adsorption.

3.3. UO_2^{2+} aqueous speciation

The aqueous speciation of UO_2^{2+} calculated using PHREEQC 3.12-8538 [41] took into account the acidic conditions and lower ionic strength ([NaCl] = 0.02 M), and the alkaline and higher ionic strength conditions ([NaCl = 0.2 M). The aqueous uranyl hydrolysis and carbonate complexation constants were implemented from the Thermochemical Databases proposed by the Nuclear Energy Agency (NEA-TDB) [53]. The solubility constant for schoepite and β-$UO_2(OH)_2$ is 5.39 (Critical Stability Constants of Metal Complexes Database, NIST Standard Reference Database 46 version 7) and 5.61 (Chemical Thermodynamics Database, NIST Standard Reference Database 2, version 1.1), respectively.

The UO_2^{2+} speciation is widely dependent on the pH conditions [58], where different complexes formed will affect the surface complexation. The distribution of aqueous species from pH 3 to pH 6, using 6.00×10^{-4} M U(VI) and 0.02 M NaCl, and from pH 5 to pH 9, using 1.00×10^{-4} M U(VI) and 0.2 M NaCl, is shown in Fig. 3. The UO_2^{2+} is the major specie up to pH 4.7, where the hydrated form will be adsorbed by smectite, whereas the formation of polynuclear species [$(UO_2)_2OH_2^{2+}$ and $(UO_2)_3OH_5^{2+}$] starts from pH 3 and 3.5, respectively. The UO_2^{2+} represents 73% of the total species at pH 4, whereas $(UO_2)_2OH_2^{2+}$ and $(UO_2)_3OH_5^{2+}$ have both proportions of 8% (Fig. 3a). The formation of $(UO_2)_4OH_7^{2+}$ species starts from pH 5 and corresponds to 15% at pH 6, where $(UO_2)_3OH_5^{2+}$ is a dominant species with a proportion of 60% (Fig. 3b).

Uranyl carbonate species start to be formed from pH 6.5 in the presence of CO_2 (g), becoming the predominant species in alkaline conditions (Fig. 3). The negative charge of uranyl carbonate complexes will compromise the adsorption on partially ionized edge sites. The UO_2^{2+} is under saturated in solution and precipitation did not occur, under the imposed conditions in batch experiments.

3.4. Modelling the sorption isotherms

The calculated isotherm parameters obtained from Langmuir, Freundlich and SIPS models are summarized in Table 3. The Freundlich isotherms revealed a good fit for lower amounts of UO_2^{2+} adsorbed (Fig. 4), confirming the heterogeneity of different energetic sites available for sorption experiments at pH 4 and pH 6. However, the experimental results are better described by Langmuir isotherm (Fig. 4) when the saturation point approaches once predicts a maximum adsorption capacity (q_m). The SIPS isotherm (Fig. 4) resulted from the Freundlich and Langmuir isotherms

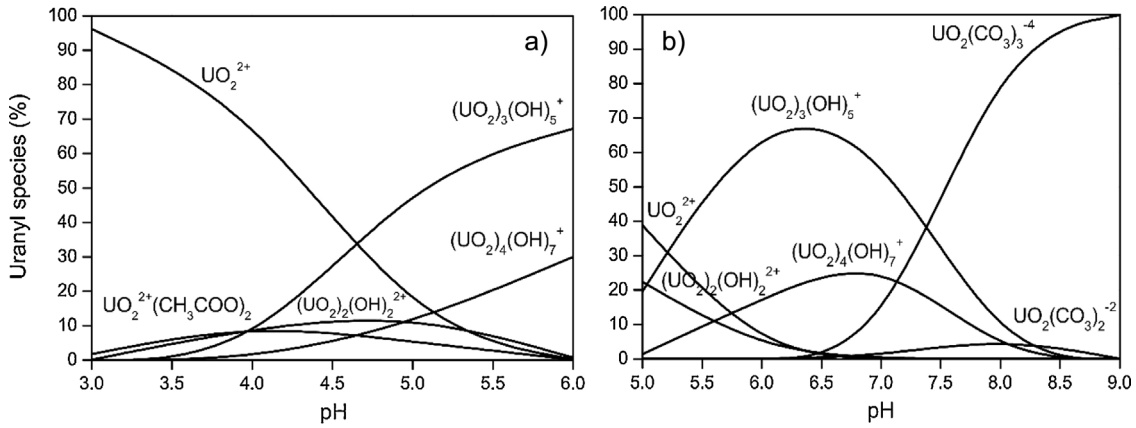

Fig. 3. Distribution of UO_2^{2+} aqueous species: a) from pH 3 to pH 6, using 6.00×10^{-4} M (UO_2^{2+}) and 1.00×10^{-2} M (NaCl) and b) from pH 5 to pH 9, using 1.00×10^{-4} M (UO_2^{2+}) and 2.00×10^{-1} M (NaCl), considering the atmospheric CO_2 effect (P = 39 Pa).

Table 3
Isotherm parameters obtained from Langmuir, Freundlich and SIPS models fit to sorption data.

Smectite	Isothermal model	Model Parameters	Sorption experiments	
			pH 4(I = 0.02 M)	pH 6 (I = 0.2 M)
BA1	Langmuir	K_L	1.03×10^4	1.07×10^6
		q_m (mol/Kg)	0.10	0.031
		r^2	0.99	0.89
	Freundlich	K_F	1.97	1.07
		N	0.41	0.31
		r^2	0.98	0.69
	SIPS	K_S	5.77×10^3	1.45×10^6
		q_m (mol/Kg)	0.12	0.027
		N	0.77	2.60
		r^2	0.99	0.99
PS2	Langmuir	K_L	1.26×10^5	1.97×10^6
		q_m (mol/Kg)	0.22	0.034
		r^2	0.99	0.94
	Freundlich	K_F	2.28	1.15
		N	0.27	0.29
		r^2	0.91	0.75
	SIPS	K_S	1.04×10^5	2.29×10^6
		q_m (mol/Kg)	0.23	0.030
		N	0.83	1.87
		r^2	0.99	0.99
PS3	Langmuir	K_L	3.14×10^4	1.32×10^6
		q_m (mol/Kg)	0.10	0.030
		r^2	0.97	0.98
	Freundlich	K_F	1.09	3.86
		N	0.30	0.40
		r^2	0.97	0.97
	SIPS	K_S	1.25×10^4	6.88×10^5
		q_m (mol/Kg)	0.13	0.038
		N	0.60	0.75
		r^2	0.99	0.99

provides the best fit of the experimental results with the higher correlation coefficients. The maximum amounts adsorbed estimated by SIPS isotherm predicts a monolayer adsorption capacity when higher UO_2^{2+} concentrations are used and the saturation point is reached. Different amounts of UO_2^{2+} were adsorbed by smectite at pH = 4 (Table 3) such as: samples BA1 and PS3 adsorbed 25% and 32% of their respective CEC, whereas sample PS2 adsorbed 44% of CEC.

Assuming that ion-exchange is the dominant adsorption mechanism under these specific conditions, three main considerations are proposed to explain the results obtained: (1) The selectivity of the exchangeable cations in the interlayer space of smectite is highly influenced by the size and valence of cation, where the preference for metal adsorption will increase as greater is the cation charge and smaller is atomic radius [59]. Both Na^+ and Ca^{2+} are exchangeable cations segregated into interlayers of smectite and the cation selectivity is a function of layer charge. The Ca^{2+} is preferentially kept in the interlayer site, while Na^+ is more easily removed by UO_2^{2+} [27] The interlayer composition of samples BA1 and PS3 have lower Na^+ compositions (43% and 50%, respectively) than sample PS2 (63%). Also, the Na^+/Ca^{2+} ratio (Table 1) reveals the major proportion of Na^+ in sample PS2, which may explain its higher capacity to adsorb UO_2^{2+} by ion-exchange. (2) The increase of tetrahedral substitution (beidellite component) reduces the distance between the adsorbed ion and the negative charge of smectite [5,6,60], producing strong interactions between UO_2^{2+} and the internal surface of smectite. The lower proportion of tetrahedral substitutions of sample PS2 favored the release of exchangeable cations from the interlayer space, enhancing the UO_2^{2+} uptake. (3) The different expansion ability of the interstratified structure (heterogeneous

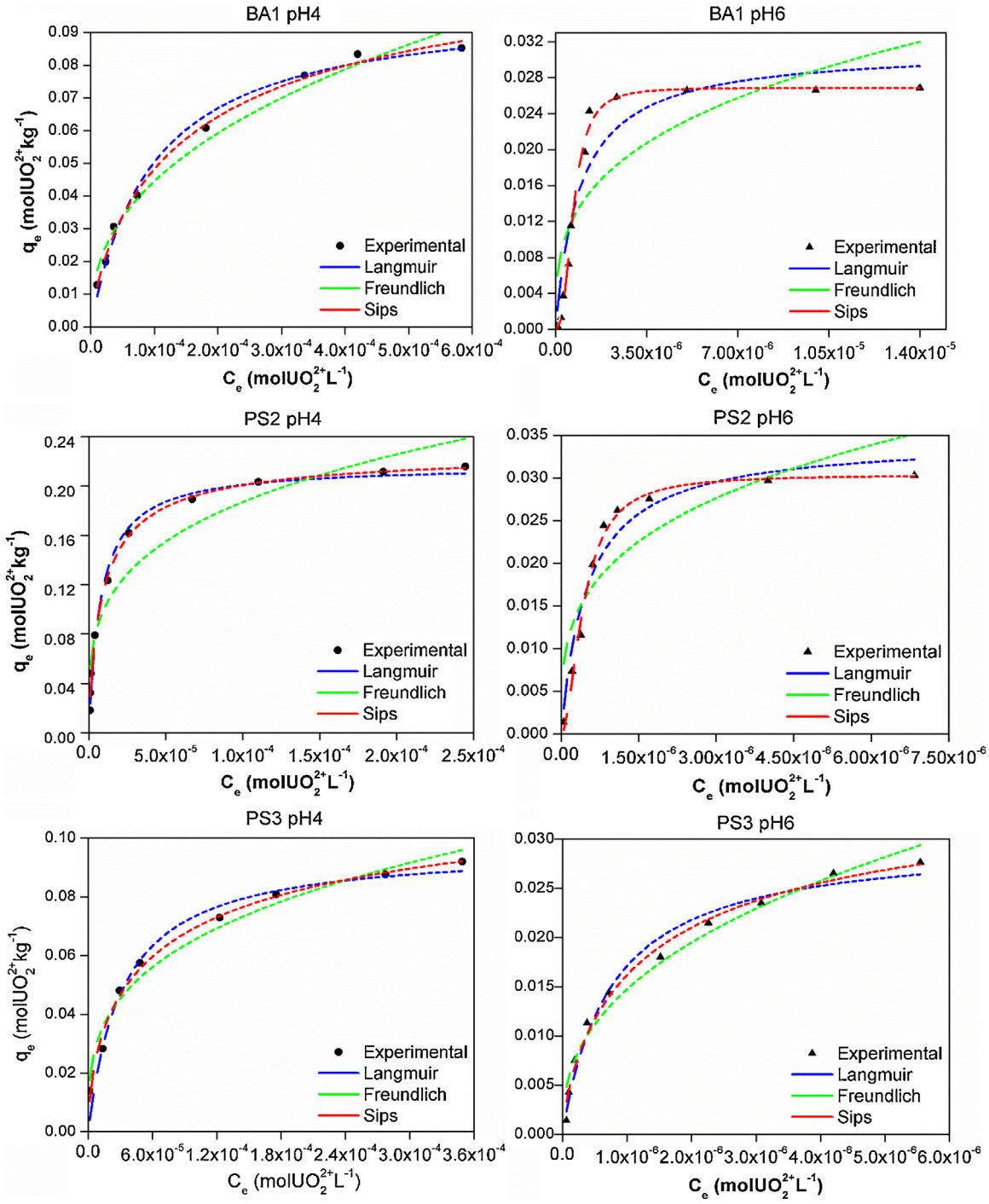

Fig. 4. Adsorption isotherms of UO_2^{2+} sorption onto heterogeneous smectite samples at pH 4 (I = 0.02 M) and pH 6 (I = 0.2 M).

character) used in sorption experiments influenced the adsorption process. Ca-smectite expands slightly limiting the contaminant diffusion, whereas Na-smectite will be completely dispersed in water enhancing the exchange process [61].

The heterogeneity factor (n) obtained from the SIPS isotherm is lower at pH = 4, indicating a lower heterogeneity of surface sites energy. Thus, the isotherms are concave (downward) and the contaminant (i.e., UO_2^{2+}) is weakly bonded to the surface if n < 1 [44,58]. In this case, it may be confirmed that UO_2^{2+} is adsorbed through weaker electrostatic interactions, when compared to that observed at pH 6, when outer-sphere complexes in the interlayer site were formed. The lower sorption affinity is also confirmed by the lower K_S values obtained (Table 3).

Adsorption on the edge sites is strongly pH-dependent due to the presence of amphoteric surface sites. The ion exchange process is inhibited at pH 6 and high ionic strength, where the adsorption occurs through the formation of UO_2^{2+} inner-sphere complexes strongly bonded onto smectite surface. The K_S also confirms this tendency (Table 3), considering the greater values obtained, indicating more favourable sorption sites. In these conditions, there is a significant decrease of the amount adsorbed (Table 3), when compared with that at pH 4, since only 10–20% of the total surface charge corresponds to the edge surface sites. However, the

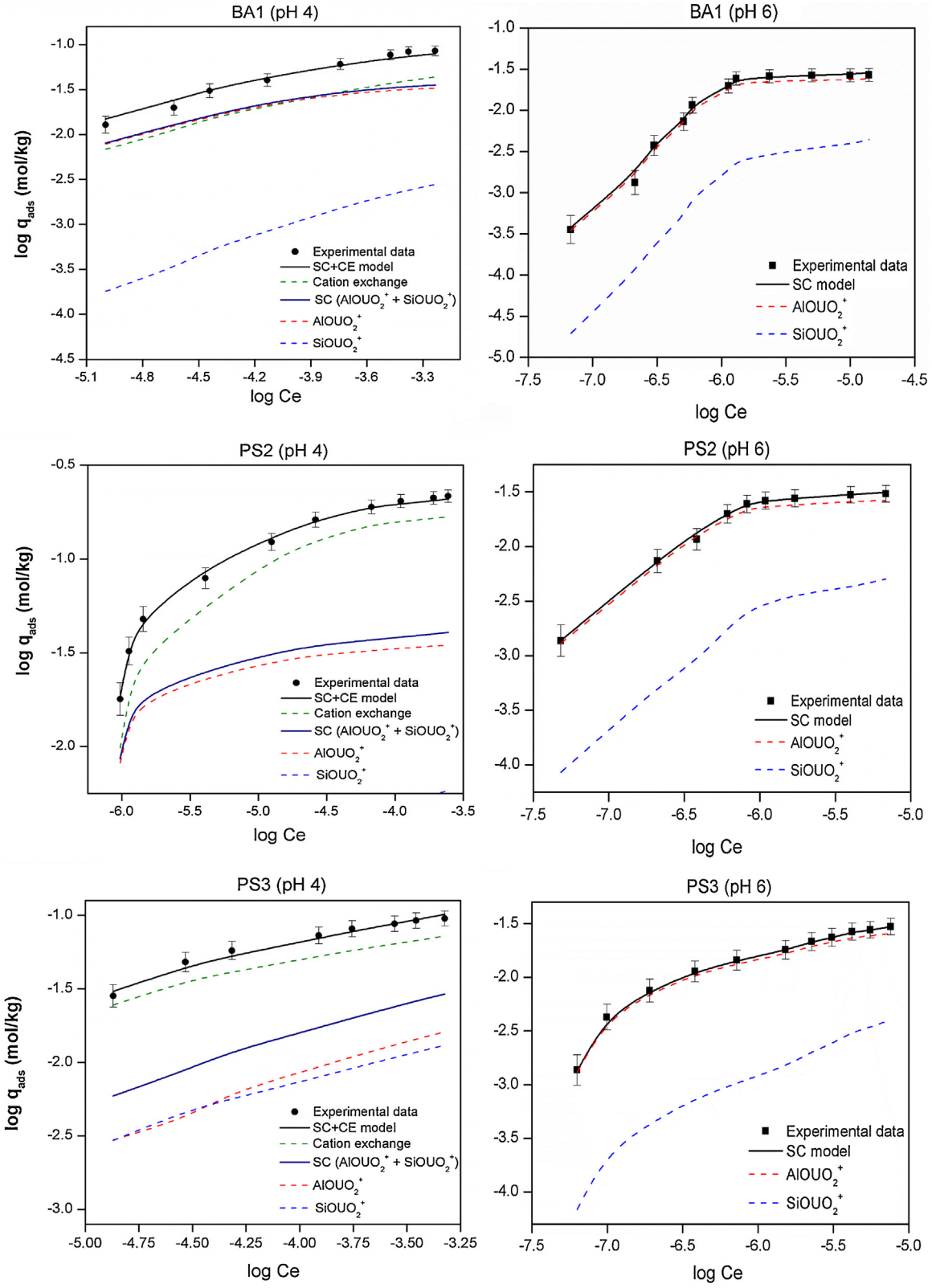

Fig. 5. Logarithm of UO_2^{2+} sorption on smectite at pH4 (I = 0.02 M) and pH 6 (I = 0.2 M) as a function of logarithm of UO_2^{2+} equilibrium concentration and simulated model.

uptake efficiency was much higher at pH 6 as increasing of UO_2^{2+} concentration, once the ratio between the amounts adsorbed per mass of smectite and the amounts of UO_2^{2+} remaining in solution at equilibrium were also significantly higher.

Taking into account the contribution of the variable charge into the total net layer charge, the edge surface sites represent 15% of the total number of available sites for sorption. In this case only 32% (sample BA1), 33% (sample PS2) and 41% (sample PS3) of the external reactive sites were completely filled by UO_2^{2+} at pH 6 (Table 3).

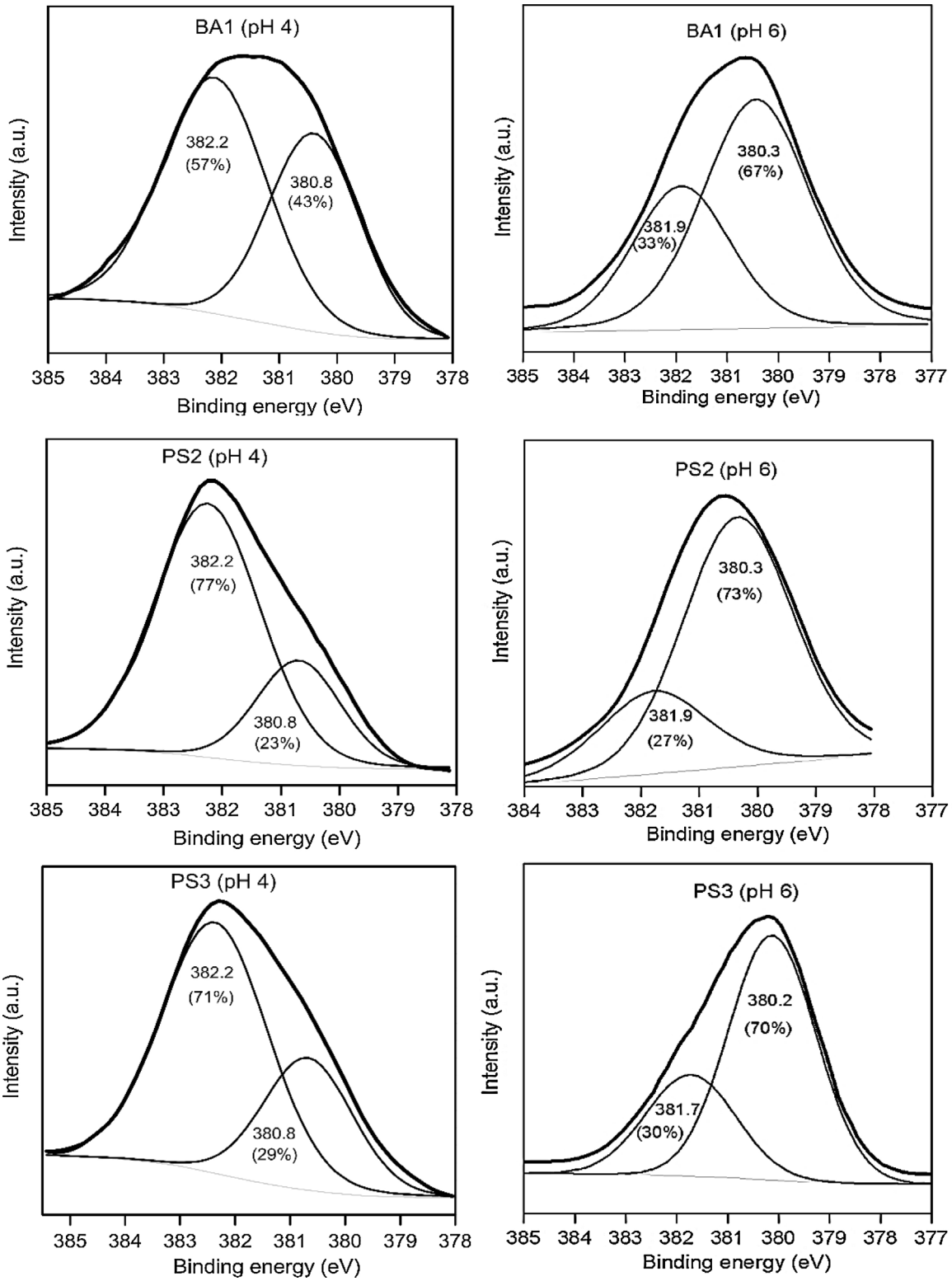

Fig. 6. The $U4f_{7/2}$ binding energy of the U(VI)-smectite samples (BA1, PS2 and PS3) obtained at pH 4 (I = 0.02 M) and pH 6 (I = 0.2 M). Fitting curves show a contribution of two components for UO_2^{2+} ions.

The obtained proportions for samples BA1 and PS2 were expected, if we take into account the overall isoelectric point of smectite.

A higher proportion of illite layers (≈30%) identified in sample PS3 results in an increase of variable charge contribution in the total charge of illite/smectite, assuming a higher ratio between the edge and the basal (total) surface area [62,63]. These structural changes affect the surface charge density of smectite, which is inversely proportional to the total number of reactive surface functional groups [34]. In this way, the adsorption on the edge surface sites has a greater influence in the total amount of UO_2^{2+} adsorbed on sample PS3 and their higher proportion of reactive sites may be associated with their lower charge density (CD = 0.59 nm^2/site), when com-

pared with samples BA1 (4.82 nm^2/site) and PS2 (2.26 nm^2/site). The higher number of reactive sites of sample PS3 justifies their higher adsorption capacity.

The increases of the energetic heterogeneity on edge surfaces, as new binding sites are formed, are suggested by the increase of the heterogeneity factors **(n)** at pH 6 (Table 3). The highly energetic sites are covered first, followed by successive occupation of sites with lower affinity. The UO_2^{2+} total concentration will define the degree of coverage of the available sites [24].

3.5. Surface complexation and cation exchange modelling

The model applied to reproduce the UO_2^{2+} adsorption on smectite was able to provide a good fit with the experimental data obtained. The model simulation and experimental data are represented by the logarithm of UO_2^{2+} sorption on smectite at pH4 (I = 0.02 M) and pH 6 (I = 0.2 M) as function of logarithm of UO_2^{2+} equilibrium concentration (Fig. 5). The RMSE values obtained at pH 4 (0.28, 0.33 and 0.40 for samples BA1, PS2 and PS3, respectively) and at pH 6, (0.06, 0.03 and 0.02) are in agreement with our experimental data obtained at both pH conditions. Accordingly, the uranyl adsorption on smectite at pH 4 could be explained by the formation of surface complexes with the permanent charged sites (UO_2X_2) and the edge surface sites such as: aluminol ($\equiv AlOUO_2^+$) and silanol ($\equiv SiOUO_2^+$) sites. The contribution of the permanent charged sites is negligible (<1%) when compared with the surface complexation onto the $\equiv AlOUO_2^+$ and $\equiv SiOUO_2^+$ sites at pH 6.

As expected, the results also reveal that the $\equiv AlOUO_2^+$ sites are more reactive than the $\equiv SiOUO_2^+$ sites, and the $\equiv AlOUO_2^+$ was the major surface species at both pH conditions. In this case, the surface complexes formed did not correspond directly to the major species detected in the U(VI) aqueous speciation, once the $\equiv AlOUO_2^+$ and $\equiv SiOUO_2^+$ occurred above the pH where UO_2^{2+} is dominant. The models described in literature [23,24,31,34] show that the UO_2^{2+} adsorption on smectite does not form a second inner-sphere complex ($\equiv SOUO_2(OH)_5$) until much higher pH values and there is no evidence that this surface complex has been adsorbed through inner-sphere complexation on the edge sites of smectite [14]. Our results revealed that the proportions of $\equiv SOUO_2(OH)_5$ species were lower than 3% for all the experiments and not represented in Fig. 5.

The proportions obtained for each sorption mechanism studied at different pH are shown in Table 4. In the case of lower UO_2^{2+} concentrations, the proportions of UO_2^{2+} adsorbed either by cation exchange or surface complexation on the edge-sites are close for the smectite samples (Fig. 5). However, the difference between both sorption mechanisms is very significant for sample PS2 as increasing of UO_2^{2+} concentration, which shows a proportion of ≈80% for cation exchange and ≈20% for surface complexation. This result confirms that cation exchange was favoured for sample PS2, where the proportion of Na^+ ions in the interlayer composition was higher and the amount of UO_2^{2+} exchanged was more significant $\left(\begin{matrix} UO_2^{2+} \\ Na^+ \end{matrix} K_C = 2.82\right)$. By contrast, sample BA1 revealed the lower ratio between the amount of UO_2^{2+} adsorbed and their cation exchange capacity and show identical proportions of UO_2^{2+} adsorbed on smectite by cation exchange and surface complexation for all the concentration range (Table 4). It confirms that the results provided by this model are in concordance with our previous conclusions, which assumed the higher proportion of Ca^{2+} in the interlayer composition and the position of negative layer charge as the main factors inhibiting the cation exchange process $\left(\begin{matrix} UO_2^{2+} \\ Ca^{2+} \end{matrix} K_C = 1.12\right)$.

Therefore, the structural changes of smectite samples, which hampers the ion-exchange process, contribute to decrease the total amount of UO_2^{2+} adsorbed but did not affect the adsorption on the edge sites of smectite, where stronger sorption complexes are formed, reducing the risk of reversibility of the UO_2^{2+} previously adsorbed.

The modelling results obtained at pH 6 indicate that the ratio between the proportion of $\equiv AlOUO_2^+$ and $\equiv SiOUO_2^+$ surface complexes increased as increasing of UO_2^{2+} concentrations. However, the proportion of surface complexes on the $\equiv AlOUO_2^+$ sites was higher than 75%, indicating a high reactivity of the $\equiv AlOUO_2^+$ sites at near-neutral pH conditions.

3.6. X-ray photoelectron spectroscopy

The XPS spectra corresponding to U4$f_{7/2}$ binding energy of UO_2^{2+} adsorbed at pH 4 and 6 on smectite (samples BA1, PS2 and PS3) are shown in Fig. 6. The atomic concentration (%) and the Si/U and Al/U atomic ratios of the studied samples after UO_2^{2+} sorption in batch experiments are shown in Table 5. The binding energies obtained after the deconvolution of the U4$f_{7/2}$ peak are shown in Table 6. Two binding energy components at 382.2 ± 0.3 eV and 380.8 ± 0.3 eV (Fig. 6) were obtained after the U4$f_{7/2}$ peak deconvolution correspond to UO_2^{2+} adsorbed on smectite at pH 4 and low ionic strength (I = 0.02 M). Two different binding energy components at 383.7 eV and 382.6 eV assigned to the $[UO_2(H_2O)_5]^{2+}$ adsorption via ion exchange onto montmorillonite (acidic conditions) and to free UO_2^{2+} sorption onto aluminol edge sites were found by other researchers [21,64]. These results are in agreement with the previous conclusions obtained by other authors, who demonstrated, using molecular spectroscopic probes, the existence of both exchange-sites and edge-sites surface complexes of UO_2^{2+} on smectite [26,58,65].

The binding energy components obtained in our work reveal the effect of structural heterogeneity of smectite samples on the UO_2^{2+} sorption behaviour. This is also supported by surface complexation and cation exchange model developed in this study. A correlation between the proportion for each binding energy component (Table 6) and the proportion of UO_2^{2+} adsorbed (%) by cation exchange and by surface complexation on the edge sites (Table 4) was obtained.

Sample PS2 reveal a major difference between cation exchange and surface complexation expressed by the following proportions of 80% and 20%. Also, a close distribution was identified concerning the proportions between high (77%) and low (23%) binding energy components. The same behavior was also verified for samples BA1, where the cation exchange process was less pronounced and the difference between the proportions of UO_2^{2+} surface species adsorbed by cation exchange (59%) and surface complexation (41%) was less significant according with the surface complexation model. Identical proportions were also confirmed by XPS results for sample BA1 where 57% was attributed to high binding energy component and 43% for the low binding energy component.

The sorption behavior of sample PS3 revealed higher sorption capacity by cation exchange than sample BA1 and lower sorption capacity than sample PS2. In this case, 72% and 71% of UO_2^{2+} was adsorbed by cation exchange through outer-sphere complexation according to the surface complexation model (Fig. 4) and the XPS results (Fig. 5), whereas 28% and 29% of UO_2^{2+} was adsorbed by surface complexation on the edge sites. Considering the concordance of both methods, we assumed that the two components detected at pH 4 are represented by the same species $[UO_2(H_2O)_5]^{2+}$, but adsorbed under different binding strengths through cation exchange and inner-sphere complexation on the edge sites of smectite.

The U4$f_{7/2}$ binding energy depends on the length of the U-O_{eq} bonds, which controls the electron density redistribu-

Table 4
Proportions of UO_2^{2+} adsorbed (%) by cation exchange and by surface complexation on the edge sites.

Sorption mechanism	BA1 (%)		PS2 (%)		PS3 (%)	
	pH 4	pH 6	pH 4	pH 6	pH 4	pH 6
Cation Exchange (UO_2X_2)	48–59[a]	<1	53–81[a]	<1	82–72[a]	<1
Surface complexation (total)	51–41[a]	99	47–19[a]	99	18–28[a]	99
$AlOUO_2^+$	98–92[a]	95–84[a]	95–86[a]	91–81[a]	48–55[a]	95–86[a]
$SiOUO_2^+$	2–8[a]	5–16[a]	5–14[a]	9–19[a]	52–45[a]	5–14[a]

[a] Variation of proportions obtained from the lower to the higher UO_2^{2+} concentrations used in different sorption experiments.

Table 5
The element composition in atomic concentration (%) and the Si/U and Al/U atomic ratios of the studied samples after UO_2^{2+} sorption in batch experiments.

pH	Samples	Atomic Concentration (%)						
		Si	O	Al	C	U	Si/U	Al/U
4	BA1	21.06	57.66	7.18	13.69	0.13	162	55
	PS2	20.56	56.84	7.18	15.08	0.17	121	42
	PS3	20.53	55.74	7.33	13.50	0.13	158	56
6	BA1	20.56	59.98	6.36	8.48	0.02	1028	318
	PS2	19.36	59.56	7.43	8.48	0.04	484	186
	PS3	19.13	60.97	7.57	8.31	0.05	383	151

Table 6
Binding energies and relative proportions of the two components fitted to U4f spectra, obtained from U(VI)-smectite samples.

Smectite	BE (eV) and relative proportions (%)			
	pH 4 (I = 0.02 M)		pH6 (0.2 M)	
	BE (eV) I	BE (eV) II	BE (eV) I	BE (eV) II
BA1	382.2 (57%)	380.8 (43%)	381.9 (33%)	380.3 (67%)
PS2	382.2 (77%)	380.8 (23%)	381.9 (27%)	380.3 (73%)
PS3	382.2 (71%)	380.8 (29%)	381.7 (30%)	380.3 (70%)

tion to or away from U(VI) centers [66,67]. The lower binding energy corresponds to strong-binding complexes onto surface and short U-O_{eq} lengths that contribute with more electron density around U(VI), enhancing the electron removal [26,66,67]. In such way, the stronger inner-sphere complexation on the aluminol and silanol sites was assigned to the lower binding energy (380.8 ± 0.3 eV), whereas the cation exchange process characterized by the weaker attraction between UO_2^{2+} and smectite surface was identified by the components appearing at higher binding energy (382.2 ± 0.3 eV).

The adsorption of UO_2^{2+} species at pH 6 and high ionic strength (I = 0.2 M) is restricted to the edge surface complexation sites, where the $\equiv AlOUO_2^+$ and $\equiv SiOUO_2^+$ are major adsorbed species [14,34]. The two new components obtained at 380.3 ± 0.3 eV and 381.8 ± 0.3 eV after U4$f_{7/2}$ peak deconvolution, correspond in fact to $\equiv AlOUO_2^+$ and $\equiv SiOUO_2^+$ species taking into account the surface complexation model developed (Table 4).

The similar proportions of each component for all the adsorbents, suggest that the structural changes did not affect significantly the adsorption behaviour when it is controlled by the reactivity of the edge surface sites. Moreover, the higher proportion observed for the component corresponding to the lower binding energy confirms the larger affinity of the $\equiv AlOUO_2^+$ sites to adsorb UO_2^{2+}. The binding strength of different complexes formed on the surface groups will depend of the attraction of the metal lattice (Al^{3+}, Mg^{2+}, Fe^{3+}, Si^{4+}), given by valence coordination number ratio values, on surface oxygen electrons: As greater is this attraction force, weaker is the attraction of the surface oxygen on the proton [68]. Although the $\equiv SiOUO_2^+$ group is primarily negatively charged at the same pH conditions, their lower tendency to donate its oxygen electrons and form inner-sphere complexes justifies the lower proportion of $\equiv SiOUO_2^+$ surface species obtained [21,65].

4. Conclusion

Smectite samples (BA1, PS2 and PS3) with a heterogeneous structure characterized by different interlayer compositions, distinct charge deficit and distribution, and interstratified structure were used in UO_2^{2+} sorption experiments at pH 4 with low ionic strength (I = 0.02 M) and pH 6 with high ionic strength (I = 0.2 M). The results obtained show that the increase of layer substitutions and the proximity between the negative charge on tetrahedral sheet and the contaminant have reduced the interlayer distances, restricting the ion-exchange process. Sample BA1 has higher tetrahedral charge than PS2 but lower cation exchange capacity, whereas sample PS3 has the higher proportion of illite interstratified layers (≈30%) and the lower number of available sites for ion-exchange. Samples BA1, PS2 and PS3 have 43%, 63% and 50% of Na^+ available for cation exchange, which adsorbed 25% (0.12 mol/kg), 44% (0.23 mol/kg) and 32% (0.10 mol/kg) of their respective CEC at pH 4. This reveals a strong competition between Ca^{2+} and UO_2^{2+} that restricted the sorption capacity mainly on sample BA1. The ion exchange was significantly reduced at pH 6 and higher ionic strength, where the amount of UO_2^{2+} adsorbed correspond to 32%, 33% and 41% of the total number of reactive external sites. Sorption capacity is related closely to the CEC, which is a function of total surface area and the smectite layer charge. The total surface area calculated increases as the mean crystal thickness distribution decreases and the CEC increases as total surface area increases. A cation exchange and surface complexation model based on diffuse double layer was successfully developed, in order to predict the UO_2^{2+} sorption on smectite. The RMSE values (%) <0.40 for all the experiments confirm a good fit to the experimental data. The modelling results showed that UO_2^{2+} was simultaneously adsorbed in the interlayer charged sites by cation exchange reaction and through inner-sphere surface complexation into the variable charged sites at pH4 (I = 0.02 M). This reveals that samples PS2 and PS3 have higher tendency to adsorb UO_2^{2+} through ion exchange, and sample BA1 has similar proportions of UO_2^{2+} absorbed by both mechanisms. The modelling results at pH 6 (I = 0.2 M) indicate that the sorption mechanism was restricted to surface complexation on the external sites of smectite where $\equiv AlOUO_2^+$ and $\equiv SiOUO_2^+$ were the major surface species. The XPS results are in agreement with the modelling obtained at both pH conditions. Two different components at 380.8 ± 0.3 and 382.2 ± 0.3 eV at pH 4 after the U4$f_{7/2}$ peak deconvolution was assigned to hydrated UO_2^{2+} adsorbed by cation exchange and by inner-sphere complexation on the external sites, respectively. Two new binding energy components at 380.3 ± 0.3 and 381.8 ± 0.3 eV identified at pH 6 correspond to $\equiv AlOUO_2^+$ and $\equiv SiOUO_2^+$ surface species, respectively.

Acknowledgements

The first author benefited a PhD scholarship (Ref. SFRH/BD/79969/2011) financed by Fundação para a Ciência e

Tecnologia (FCT), Portugal. This work was funded by FEDER fund through the Operational Program Competitiveness Factors and COMPETE. The financial support of project P12-RNM-1565 from Junta de Andalucia and FEDER funds is also acknowledged. The first author thanks to Dr. Maria Marques Fernandes and Dr. Bart Baeyens for very fruitful, constructive discussions on this topic and friendly accompany during the work in the Paul Scherrer Institute—Villigen, CH. The authors thank to Dr. Gianluca Li Puma for editorial handling and to the three anonymous reviewers for excellent critical review, helpful suggestions and for thorough reading of the initial manuscript.

Appendix A. Supplementary data

Supplementary data associated with this article can be found, in the online version, at http://dx.doi.org/10.1016/j.jhazmat.2016.05.060.

References

[1] R. Pusch, J. Kasbohm, S. Knutsson, T. Yang, L. Nguyen-Thanh, The role of smectite clay barriers for isolating high-level radioactive waste (HLW) in shallow and deep repositories, Procedia Earth Planet. Sci. 15 (2015) 680–687.
[2] A. Meunier, D. Proust, D. Beaufort, A. Lajudie, J.C. Petit, Heterogeneous reactions of dioctahedral smectites in illite-smectite and kaolinite-smectite mixed-layers: applications to clay materials for engineered barriers, Appl. Geochem. 1 (1992) 143–150.
[3] J.O. Lee, I.M. Kang, W.J. Cho, Smectite alteration and its influence on the barrier properties of smectite clay for a repository, Appl. Clay Sci. 47 (2010) 99–104.
[4] G.E. Christidis, A.E. Blum, D.D. Eberl, Influence of layer charge and charge distribution of smectites on the flow behaviour and swelling of bentonites, Appl. Clay Sci. 34 (2006) 125–138.
[5] E. Ferrage, B. Lanson, B.A. Sakharov, V.A. Drits, Investigation of smectite hydration properties by modeling experimental X-ray diffraction patterns: part I: montmorillonite hydration properties, Am. Mineral. 90 (2005) 1358–1374.
[6] E. Ferrage, B. Lanson, B.A. Sakharov, N. Geoffroy, E. Jacquot, V.A. Drits, Investigation of dioctahedral smectite hydration properties by modeling of X-ray diffraction profiles: influence of layer charge and charge location, Am. Mineral. 92 (2007) 1731–1743.
[7] B. Dazas, B. Lanson, A. Delville, J.L. Robert, S. Komarneni, L.J. Michot, E. Ferrage, Influence of tetrahedral layer charge on the organization of interlayer water and ions in synthetic Na-saturated smectites, J. Phys. Chem. C 119 (2015) 4158–4172.
[8] D.A. Laird, Influence of layer charge on swelling of smectites, Appl. Clay Sci. 34 (2006) 74–87.
[9] D. Proust, J. Lechelle, A. Meunier, A. Lajudie, Hydrothermal reactivity of mixed-layer kaolinite/smectite and implications for radioactive waste disposal, Eur. J. Mineral. 2 (1990) (1990) 313–325.
[10] A. Bouchet, D. Proust, A. Meunier, D. Beaufort, High-charge to low-charge smectite reaction in hydrothermal alteration processes, Clay Miner. 23 (1988) 133–146.
[11] D.D. Eberl, The reaction of montmorillonite to mixedlayer clay: the effect of interlayer alkali and alkaline earth cations, Geochim. Cosmochim. Acta 42 (1978) 1–7.
[12] A. Inoue, M. Utada, K. Wakita, Smectite-to-illite conversion in natural hydrothermal systems, Appl. Clay Sci. 7 (1992) 131–145.
[13] I. Grenthe, J. Fuger, R. Konings, R.J. Lemire, C. Nguyen-Trung, A.B. Muller, J. Wanner, The Chemical Thermodynamics of Uranium, Elsevier, 1992, pp. 717.
[14] C.J. Chisholm-Brause, J.M. Berg, R.A. Matzner, D.E. Morris, Uranium(VI) sorption complexes on montmorillonite as a function of solution chemistry, J. Colloid Interface Sci. 233 (2001) 38–49.
[15] E.A. Hudson, L.J. Terminello, B.E. Viani, M.A. Denecke, T. Reich, P.G. Allen, J.J. Bucher, D.K. Shuh, N.M. Edelstein, The structure of U^{6+} sorption complexes on vermiculite and hydrobiotite, Clays Clay Miner. 47 (1999) 439–457.
[16] B. Campos, J. Aguilar-Carrillo, M. Algarra, M.A. Gonçalves, E. Rodríguez-Castellón, J.C.G. Esteves da Silva, I. Bobos, Adsorption of uranyl ions on kaolinite montmorillonite, humic acid and composite clay material, Appl. Clay Sci. 85 (2003) 53–63.
[17] J.G. Catalano, G.E. Brown Jr., Uranyl adsorption onto montmorillonite: evaluation of binding sites and carbonate complexation, Geochim. Cosmochim. Acta 69 (2005) 2995–3005.
[18] C. Hennig, T. Reich, R. Dahn, A.M. Scheidegger, Structure of uranium sorption complexes at montmorillonite edge sites, Radiochim. Acta 90 (2002) 653–657.
[19] S.P. Hyun, Y.H. Cho, P.S. Hahn, S.J. Kim, Sorption mechanism of U(VI) on a reference montmorillonite: binding of the internal and external surfaces, J. Radioanal. Nucl. Chem. 250 (2001) 55–62.
[20] S.J. Kim, Sorption mechanism of U(VI) on a reference montmorillonite: binding to the internal and external surfaces, J. Radioanal. Nucl. Chem. 250 (2001) 55–62.
[21] A. Kowal-Fouchard, R. Drot, E. Simoni, J.J. Ehrhardt, Use of spectroscopic techniques for uranium(vi)/montmorillonite interaction modeling, Environ. Sci. Technol. 38 (2004) 1399–1407.
[22] M. Marques-Fernandes, B. Baeyens, P. Dähn, A.C. Scheinost, M.H. Bradbury, U(VI) sorption on montmorillonite in the absence and presence of carbonate: a macroscopic and microscopic study, Geochim. Cosmochim. Acta 93 (2012) 262–277.
[23] J.P. McKinley, M. Zachara, S.C. Smith, G.D. Turner, The influence of hydrolysis and multiple site-binding reactions on adsorption of U(VI) to montmorillonite, Clays Clay Miner. 43 (1995) 586–598.
[24] R.T. Pabalan, D.R. Turner, Uranium(VI) sorption on montmorillonite: experimental and surface complexation modeling study, Aquat. Geochem. 2 (1997) 203–226.
[25] M.L. Schlegel, M. Descontes, Uranium uptake by hectorite and montmorillonite: a solution chemistry and polarized EXAFS study, Environ. Sci. Technol. 43 (2009) 8593–8598.
[26] E.R. Sylwester, E.A. Hudson, P.G. Allen, The structure of uranium (VI) sorption complexes on silica alumina, and montmorillonite, Geochim. Cosmochim. Acta 64 (2000) 2431–2438.
[27] A. Tsunashima, G.W. Brindley, M. Bastovanov, Adsorption of uranium from solutions by montmorillonite; compositions and properties of uranyl montmorillonites, Clays Clay Miner. 29 (1981) 10–16.
[28] J.A. Greathouse, R.T. Cygan, Water structure and aqueous uranyl (VI) adsorption equilibria onto external surfaces of beidellite montmorillonite, and pyrophyllite: results from molecular simulations, Environ. Sci. Technol. 40 (2006) 3865–3871.
[29] A. Bauer, T. Schafer, R. Dohrmann, H. Hoffmann, J.I. Kim, Smectite Stability in acid salt solutions and the fate of Eu, Th and U in solution, Clay Miner. 36 (2001) 93–103.
[30] D.M. Giaquinta, L. Soderhom, S.E. Yuchs, S.R. Wasserman, The speciation of uranium in smectite clay: evidence for catalyzed uranyl reduction, Radiochim. Acta 76 (1997) 113–121.
[31] S. Korichi, A. Bensmaili, Sorption of uranium (VI) on homoionic sodium smectite experimental study and surface complexation modeling, J. Hazard. Mater. 169 (2009) 780–793.
[32] M.T. Olguin, M. Solache-Rios, D. Acosta, P. Bosch, S. Bulbulian, UO_2^{2+} sorption on bentonite, J. Radioanal. Nucl. Chem. 218 (1997) 65–69.
[33] M. Schindler, C.A. Legrand, M.F. Hochella Jr., 2015. Alteration: adsorption and nucleation processes on clay–water interfaces: mechanisms for the retention of uranium by altered clay surfaces on the nanometer scale, Geochim. Cosmochim. Acta 153 (2015) 15–36.
[34] D.R. Turner, S.A. Sassman, Approaches to sorption modeling for high-level waste performance assessment, J. Contam. Hydrol. 21 (1996) 311–332.
[35] S.J. Kim, Sorption mechanism of U(VI) on a reference montmorillonite: binding to the internal and external surfaces, J. Radioanal. Nucl. Chem. 250 (2001) 55–62.
[36] J.M. Zachara, J.P. McKinley, Influence of hydrolysis on the sorption of metal cations by smectites: importance of edge coordination reactions, Aquat. Sci. 55 (1993) 250–261.
[37] M.H. Bradbury, B. Baeyens, Modelling the sorption of Mn(II), Co(II), Ni(II), Zn(II), Cd(II), Eu(III), Am(III), Sn(IV), Th(IV), Np(V) and U(VI) on montmorillonite: linear free energy relationships and estimates of surface binding constants for some selected heavy metals and actinides, Geochim. Cosmochim. Acta 69 (22) (2005) 875–892.
[38] R.T. Pabalan, F.P. Bertetti, J.D. Prikryl, D.R. Turner, Uranium (VI) sorption onto selected mineral surfaces: key geochemical parameters, Abstr. Am. Chem.l Soc. 211 (1995) 55–Geoc.
[39] G.D. Turner, J.M. Zachara, J.P. McKinley, S.C. Smith, Surface-charge properties and UO_2^{2+} adsorption of a subsurface smectite, Geochim. Cosmochim. Acta 60 (1996) 3399–3414.
[40] V. Guimarães, E. Rodríguez-Castellón, M. Algarra, F. Rocha, I. Bobos, Kinetics of uranyl ions sorption on heterogeneous smectite structure at pH 4 and 6 using a continuous stirred flow-through reactor, Appl. Clay Sci. (2016) (in press).
[41] D.L. Parkhurst, C.A.J. Appelo, A computer program for speciation, batch-reaction, one-dimensional transport, and inverse geochemical calculations, Description of input and examples for PHREEQC version 3, U.S. Geological Survey Techniques and Methods (2013) p497.
[42] I. Langmuir, The constituition and fundamental properties of solids and liquids. Part I, Solids J. Am. Chem. Soc. 38 (1916) 2221–2295.
[43] H. Chen, A. Wang, Kinetic and isothermal studies of lead ion adsorption onto palygorskite clay, J. Colloid Interface Sci. 307 (2007) 309–316.
[44] R.P. Schwarzenbach, P.M. Gschwend, D.M. Imboden, Environmental Organic Chemistry, Wiley, 2005, pp. 1000.
[45] S. Maurer, Prediction of Single Component Adsorption Equilibria Ph.D. Thesis, TU München (Herbert Utz, Wissenschaft, München), 2000.
[46] G.P. Jeppu, T.P. Clement, A modified Langmuir-Freundlich isotherm model for simulating pH-dependent adsorption effects, J. Contam. Hydrol. 129–130 (2012) 46–53.
[47] S. Bachmaf, B. Merkel, Estimating water chemistry parameters from experimental data using PEST with PHREEQC, FOG—Freiberg Online Geol. 28 (2011) 1–18.
[48] M.H. Bradbury, B. Baeyens, Sorption modelling on illite Part I: titration measurements and the sorption of Ni, Co, Eu and Sn, Geochim. Cosmochim. Acta 73 (2009) 990–1003.

[49] M.H. Bradbury, B. Baeyens, A generalised sorption model for the concentration dependent uptake of caesium by argillaceous rocks, J. Contam. Hydrol. 42 (2000) 141–163.
[50] C. Tournassat, E. Ferrage, C. Poinsignon, L. Charlet, The titration of clay minerals: II. Structure-based model and implications for clay reactivity, J. Colloid Interface Sci. 273 (2004) 234–246.
[51] S.J. Anderson, G. Sposito, Cesium-adsorption method for measuring accessible structural surface charge, Soil Sci. Soc. Am. J. 55 (1991) 1569–1576.
[52] G.N. White, L.W. Zelazny, Analysis and implications of the edge structure of dioctahedral phyllosilicates, Clays Clay Miner. 36 (1988) 141–146.
[53] R. Guillaumont, T. Fanghänel, J. Fuger, I. Grenthe, V. Neck, D.-A. Palmer, M.H. Rand, Update on the Chemical Thermodynamics of Uranium, Neptunium, Plutonium, Americium and Technetium, Elsevier Science, 2003, pp. p715.
[54] H. Wanner, I. Forest, in: O.N.E (Ed.), Chemical Thermodynamics of Uranium, In: Agency, Data Bank Issy-les-Moulineaux France, 1992.
[55] A.L. Herbelin, J.C. Westall, FITEQL 4.0: A Computer Program for Determination of Chemical Equilibrium Constants from Experimental Data; Report 99-01, Department of Chemistry, Oregon State University Corvallis, 1999.
[56] D.S. Powlson, P. Smith, J.U. Smith, Evaluation of Soil Organic Matter Models: Using Existing Long-Term Datasets, Springer-Verlag, Heidelberg, 2013.
[57] V. Drits, D.D. Eberl, J. Środoń, XRD measurement of mean thickness: thickness distribution and strain for illite and illite-smectite crystallites by the Bertaut-Warren-Averbach technique, Clays Clay Miner. 46 (1998) 38–50.
[58] C. Chisholm-Brause, S.D. Conradson, C.T. Buscher, P.G. Eller, D.E. Morris, Speciation of uranyl sorbed at multiple binding sites on montmorillonite, Geochim. Cosmochim. Acta 58 (1994) 3625–3631.
[59] J. Wilson, Rock-Forming Minerals: Sheet Silicates: Clay Minerals Volume 3C, Geological Society of London, 2013.
[60] S.L. Teich-McGoldrick, J.A. Greathouse, C.F. Jové-Colón, R.T. Cygan, Swelling properties of montmorillonite and beidellite clay minerals from molecular simulation: comparison of temperature interlayer cation, and charge location effects, J. Phys. Chem. C 119 (2015) 20880–20891.
[61] W.K. Dorfner, Ion Exchangers, Walter de Gruyter, Berlin and New York, 1991.
[62] D. Vallero, Environmental contaminants: assessment and control, Elsevier Science, 2010, pp. p801.
[63] P.M. Huang, Y. Li, M.E. Sumner, Handbook of soil sciences: properties and processes, Second edition, Taylor & Francis, 2011, pp. p1442.
[64] R. Drot, J. Roques, E. Simoni, Molecular approach of the uranyl/mineral interfacial phenomena, Comptes Rendu de Chimie 10 (2007) 1078–1091.
[65] D.E. Morris, C.J. Chisholm-Brause, M.E. Barr, S.D. Conradson, Optical spectroscopic studies of the sorption of UO_2^{2+} species on a reference smectite, Geochim. Cosmochim. Acta 58 (1994) 3613–3623.
[66] M. Del Nero, A. Froideval, C. Gaillard, G. Mignot, R. Barillon, L. Monier, A. Ozgümüs, Mechanisms of uranyl sorption, 236, Geological Society London, Special Publications, 2004, pp. 545–560.
[67] E.S. Ilton, P.S. Bagus, XPS determination of uranium oxidation states, Surf. Interface Anal. 43 (2004) 1549–1560.
[68] A. Froideval, M. Del Nero, R. Barillon, J. Hommet, G. Mignot, dependence of uranyl retention in a quartz/solution system: an XPS study, J. Colloid Interface Sci. 266 (2003) 221–235.